Editors' Suggestion

Ultra-Large-Scale Deterministic Entanglement Containing $2 \times 20\,400$ Optical Modes Based on Time-Delayed Quantum Interferometer

Yanfen Zhou,[1,*] Wei Wang,[1,*] Tingting Song,[1] Xutong Wang,[1] Qiqi Zhu,[1] Kai Zhang,[1] Shengshuai Liu,[1,†] and Jietai Jing[1,2,3,‡]

[1]*State Key Laboratory of Precision Spectroscopy, Joint Institute of Advanced Science and Technology, School of Physics and Electronic Science, East China Normal University, Shanghai 200062, China*
[2]*CAS Center for Excellence in Ultra-intense Laser Science, Shanghai 201800, China*
[3]*Collaborative Innovation Center of Extreme Optics, Shanxi University, Taiyuan, Shanxi 030006, China*

(Received 24 March 2022; revised 24 October 2022; accepted 18 January 2023; published 7 February 2023)

Quantum entanglement is an indispensable resource for implementing quantum information processing. The scale of quantum entanglement directly determines its quantum information processing capability. Therefore, it is of great importance to generate ultra-large-scale (ULS) quantum entanglement for the development of quantum information science and technology. Many efforts have been made to increase the scale of quantum entanglement. Recently, time-domain multiplexing has been introduced into continuous-variable (CV) quantum systems to greatly enlarge the scale of quantum entanglement. In this Letter, based on a time-delayed quantum interferometer, we theoretically propose and experimentally demonstrate a scheme for generating an ULS CV deterministic entanglement containing $2 \times 20\,400$ optical modes. In addition, such ULS entanglement contains 81 596 squeezed modes. Our results provide a new platform for implementing ULS CV quantum information processing.

DOI: 10.1103/PhysRevLett.130.060801

Quantum entanglement [1] as an essential quantum resource plays an important role in both fundamental research and quantum information technology [2], especially in quantum computation [3–9], quantum communication [10–15], and quantum metrology [16–18]. Since quantum entanglement was applied to quantum information, more and more attention has been paid to expanding the scale of quantum entanglement [19–24]. To generate ultra-large-scale (ULS) quantum entanglement, it is crucial to find an efficient way to boost the scale of quantum entanglement. In this aspect, integrating multiple nonlinear processes into a single device is a promising way to efficiently enhance the scale of the continuous-variable (CV) deterministic entanglement. For instance, multicolor entanglement is generated by wavelength multiplexing [25], a 60-mode dual-rail cluster state is produced by quantum optical frequency comb [26], and a large-scale quantum network is constructed by orbital angular momentum optical mode [27]. In addition, the concept of time-domain multiplexing has recently been introduced into CV quantum systems to greatly enlarge the scale of quantum entanglement [28–31]. These ULS CV entangled states are promising for implementing ULS CV quantum information processing.

Here, we theoretically propose and experimentally demonstrate a scheme for efficiently generating an ULS CV quantum entanglement with state structure different from the works of other groups [28–31] based on a time-delayed SU(1,1) quantum interferometer. An SU(1,1) quantum interferometer [32,33] consists of two parametric amplifiers based on either a four-wave mixing (FWM) process or a parametric down-converter, which can beat the classical interferometer in terms of phase sensitivity [34,35]. In our scheme, the first FWM process of the quantum interferometer serves as the entangled source. Then we introduce a time-delay line by an optical fiber in one of the two arms of the quantum interferometer, which realizes the function of time multiplexing. Finally, we exploit the secondary FWM process of the SU(1,1) quantum interferometer to realize the combination of the time-delayed entangled beams. As a result, an ULS CV quantum entanglement of $2 \times 20\,400$ modes with state structure different from the works of other groups [28–31] is generated from such time-delayed SU(1,1) quantum interferometer. Our results provide a new platform for implementing ULS CV quantum information processing.

The schematic of a time-delayed SU(1,1) quantum interferometer for generating ULS CV quantum entanglement is shown in Fig. 1(a) where two FWM processes occur in two 12-mm-long ^{85}Rb vapor cells whose temperatures are stabilized at around 116 °C. The FWM process is based on the double-Λ energy level configuration of the $D1$ line of ^{85}Rb as shown in Fig. 1(b). In the FWM process, a high-intensity pump beam with a frequency of about 377.110 10 THz drives an off-resonant transition, and the atom in the ground state $(5S_{1/2}, F = 2)$ will transit to the virtual state $|2\rangle$ which is 0.95 GHz, called one-photon detuning (Δ), away from the excited state $(5P_{1/2})$. Under

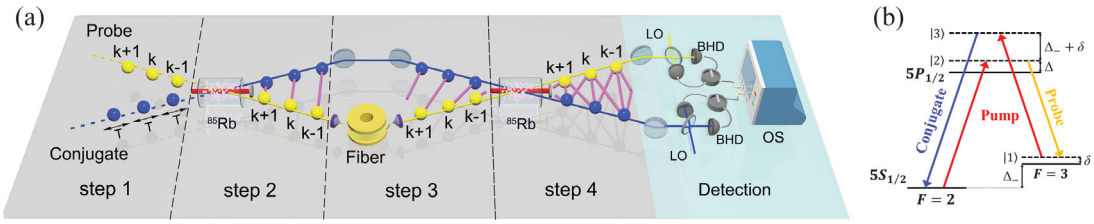

FIG. 1. Generating ULS CV quantum entanglement based on a time-delayed SU(1,1) quantum interferometer. (a) Experimental schematic. The yellow and blue spheres represent the time wave packets of probe beam and conjugate beam with time duration T, respectively. The whole process can be divided into four steps. The time delay caused by optical fiber is equal to T. The magenta links represent the interaction of optical wave packets. …, $k-1, k, k+1, \ldots$ stand for the time wave packet index. LO, local oscillator; BHD, balanced homodyne detection; OS, oscilloscope. (b) The double-Λ energy level configuration of the $D1$ line of ^{85}Rb. Δ, one-photon detuning; δ, two-photon detuning; Δ_-, the ^{85}Rb ground-state hyperfine splitting.

the action of Stokes scattering, the atom will transit to the virtual state $|1\rangle$ which is 4 MHz, called two-photon detuning (δ), away from the ground state $(5S_{1/2}, F = 3)$. At the same time, a probe photon, whose frequency is $\Delta_- + \delta$ lower than the pump beam, is produced. Here, Δ_- is the ^{85}Rb ground-state hyperfine splitting of 3.036 GHz. Then, the atom is pumped to the virtual state $|3\rangle$. Because of the action of anti-Stokes scattering, the atom will return to the ground state $(5S_{1/2}, F = 2)$. At the same time, a conjugate photon, whose frequency is $\Delta_- + \delta$ higher than the pump beam, is produced. Therefore, a probe beam with a frequency of $\Delta_- + \delta$ redshifted and a conjugate beam with a frequency of $\Delta_- + \delta$ blueshifted from the pump beam are simultaneously generated in the FWM process. Firstly, the probe beam (yellow dotted line) whose power is about 0.5 μW and the conjugate beam in vacuum state (blue dotted line) are simultaneously and symmetrically crossed with a strong pump beam (red straight line) at the center of the first ^{85}Rb vapor cell. The pump beam is vertically polarized, while the probe and conjugate beams are horizontally polarized. We divide each beam into time bins of time period T and define such a time bin as a time wave packet (step 1), where T is about 140 ns and greater than the coherence time of the FWM process [36,37]. Here, the time duration of each wave packet is equal to the time interval of the wave packet. Such wave packets denoted by the yellow or blue spheres are mutually independent and separated from each other in time (see the Supplemental Material for details [38]). Secondly, the first FWM process of quantum interferometer deterministically creates a series of entangled states separated by time interval of T (step 2). We mark the probe (conjugate) beam as pr (conj) and denote the interaction strength of this process by parameter β, which is highly dependent on the power of pump beam, one-photon detuning, and two-photon detuning, then the interaction Hamiltonian can be written as

$$\hat{H} = i\hbar \sum_{1}^{k} \beta \hat{a}_{\mathrm{pr},k}^{(2)\dagger} \hat{a}_{\mathrm{conj},k}^{(2)\dagger} + \mathrm{H.c.}, \tag{1}$$

where $\hat{a}_{\mathrm{pr},k}^{(2)\dagger}$ and $\hat{a}_{\mathrm{conj},k}^{(2)\dagger}$ represent the creation operators of the kth wave packet of the probe and conjugate beams, respectively, which are generated by the first FWM process, and integer k represents the index of time wave packet, $k \in [1, 20\,400]$. H.c. is the Hermitian conjugate. The interaction by the first FWM process is represented by magenta links between blue and yellow spheres in step 2. The generated states in step 2 can be expressed as

$$\begin{aligned} \hat{a}_{\mathrm{conj},k}^{(2)} &= \sqrt{G_1}\hat{a}_{\mathrm{conj},k}^{(1)} + \sqrt{G_1 - 1}\hat{a}_{\mathrm{pr},k}^{(1)\dagger}, \\ \hat{a}_{\mathrm{pr},k}^{(2)} &= \sqrt{G_1 - 1}\hat{a}_{\mathrm{conj},k}^{(1)\dagger} + \sqrt{G_1}\hat{a}_{\mathrm{pr},k}^{(1)}, \end{aligned} \tag{2}$$

where $G_1 = \cosh^2(\beta\tau_1)$ is the gain of the first FWM process, τ_1 is the mixing interaction time. $\hat{a}_{\mathrm{pr},k}^{(1)\dagger}$ ($\hat{a}_{\mathrm{pr},k}^{(1)}$) and $\hat{a}_{\mathrm{conj},k}^{(1)\dagger}$ ($\hat{a}_{\mathrm{conj},k}^{(1)}$) are the creation (annihilation) operators of the kth wave packet of the input probe and conjugate beams from step 1, respectively. The specific evolution process of Eq. (2) is described in the Supplemental Material [38]. Thirdly, the yellow spheres of the probe beam are delayed for the time duration T of about 140 ns, which we choose as the time duration T of the wave packet, after passing through an optical fiber delay line with a length of 30 m and an insertion loss of about 10% (step 3). After such time delay, each yellow sphere of entangled states is synchronized in time with each blue sphere of successive entangled states. The relation between time wave packets of step 3 and step 2 is given by

$$\begin{aligned} \hat{a}_{\mathrm{conj},k}^{(3)} &= \hat{a}_{\mathrm{conj},k}^{(2)}, \\ \hat{a}_{\mathrm{pr},k}^{(3)} &= \hat{a}_{\mathrm{pr},k-1}^{(2)}. \end{aligned} \tag{3}$$

After step 3, a series of entangled states staggered in time are generated. Fourthly, by combining the staggered entangled states on the second FWM process of quantum interferometer, each blue sphere of conjugate beam and each yellow sphere of probe beam synchronized in time will interact with each other (step 4). Such interaction will directly lead to the magenta interaction links of blue and yellow spheres in the

vertical direction, i.e., the link of the kth blue and yellow spheres in step 4. Meanwhile, due to the nonlinear interactions from the first and second FWM processes, each yellow (blue) sphere contains the information of the blue (yellow) sphere of the previous step, which makes the diagonal magenta interaction links of wave packets in step 4. Therefore, each wave packet of conjugate (probe) beam will connect to three most neighboring wave packets of probe (conjugate) beam by the magenta interaction links. By using G_2 to represent the gain of the second FWM process, the final output states can be expressed as

$$\hat{a}^{(4)}_{\mathrm{pr},k} = \sqrt{G_2}\hat{a}^{(3)}_{\mathrm{pr},k} + e^{i\varphi}\sqrt{G_2-1}\hat{a}^{(3)\dagger}_{\mathrm{conj},k},$$
$$\hat{a}^{(4)}_{\mathrm{conj},k} = e^{i\varphi}\sqrt{G_2-1}\hat{a}^{(3)\dagger}_{\mathrm{pr},k} + \sqrt{G_2}\hat{a}^{(3)}_{\mathrm{conj},k}. \quad (4)$$

Here, $\varphi = 2\varphi_c$, where φ_c is the phase of the pump beam of the second ^{85}Rb vapor cell. The input-output relation of the whole time-delayed SU(1,1) quantum interferometer is given in the Supplemental Material [38]. The beam propagation efficiency after each FWM process by taking into account the atomic absorption and the losses of optical elements (the fiber insertion loss is counted separately) is about 90%; therefore, it introduces propagation loss of about 10%.

For our system, the quantum properties of the generated state can be acquired by balanced homodyne detection (BHD) technique. The signal field can be projected onto a specific mode which has the same frequency with the bright local oscillator (LO). Here, the LOs are obtained by setting up a similar setup a few millimeters above the current corresponding beams [41] (see the Supplemental Material for details [38]). Specifically, by BHD, we can get the quantum fluctuations of the generated state's amplitude quadrature $\hat{X}$ and phase quadrature $\hat{Y}$ which can be conveniently organized in the form of a covariance matrix (CM) [42]. Then, positivity under partial transposition criterion can be used to verify the entanglement [43,44]. We take $\hat{a}^{(4)}_{\mathrm{pr},k}$, $\hat{a}^{(4)}_{\mathrm{conj},k}$, $\hat{a}^{(4)}_{\mathrm{pr},k+1}$, and $\hat{a}^{(4)}_{\mathrm{conj},k+1}$ as a unit to investigate the multipartite entanglement of these four wave packets and there are 20 399 such wave packet units for our experiment in total. For such a wave packet unit, it contains two kinds of possible partial transposed operations of 1×3 and 2×2 [45], which results in seven possible bipartitions [46] (see the Supplemental Material for details [38]). If all the symplectic eigenvalues v of the seven bipartitions are smaller than 1 for each wave packet unit, then we can claim that the ULS CV quantum entanglement containing $2\times 20\,400$ modes is generated in our system. Moreover, a smaller v indicates a stronger entanglement strength. It can be found that for each generated wave packet unit, its smallest symplectic eigenvalues v of the seven bipartitions depend on the internal phase φ of the time-delayed SU(1,1) quantum interferometer (see the Supplemental Material for details [38]). When $\varphi = n\pi$ (n is an integer), all seven v find their minima. Therefore, in the experiment, we choose to lock φ at 0 by a microcontrol unit [47]. The visibility of SU(1,1) quantum interferometer can reach about 97%, which is critical for our experiment because low visibility will introduce extra noise and then deteriorate the entanglement. For two BHDs, the relative phases between signal beams and the corresponding LOs also need to be locked in order to measure the desired field quadratures. Specifically, when the relative phase is locked to 0 ($\pi/2$), we are able to measure the amplitude (phase) quadratures $\hat{X}^{(4)}_{\mathrm{pr},k}$ and $\hat{X}^{(4)}_{\mathrm{conj},k}$ ($\hat{Y}^{(4)}_{\mathrm{pr},k}$ and $\hat{Y}^{(4)}_{\mathrm{conj},k}$). The visibility of each BHD is about 98% and the photodetector of each BHD has a quantum efficiency of about 97%. In order to avoid the effect of laser noise of the initial seeding probe beam on the measurement results, the data are acquired when the initial seeding probe beam is blocked with a vacuum locking technique (see the Supplemental Material for details [38]). All the photocurrents from BHDs are recorded by a digital oscilloscope (OS). The sampling rate of the OS is set to 100 MHz in order to take enough data points for each wave packet, and each frame of 100 ms contains 1×10^7 data points. We divide each frame into 35 segments and each segment contains about 20 400 wave packets which construct 20 399 wave packet units. For each quadrature measurement of wave packets we measure 100 frames, and thus we can get 3500 segments to calculate the variances of amplitude quadrature $\hat{X}$ and phase quadrature $\hat{Y}$ of wave packets. In this way, we can get the information of amplitude and phase quadratures of $2\times 20\,400$ time wave packets.

Figure 2(a) shows the smallest symplectic eigenvalues of 20 399 wave packet units when $G_1 = 1.3$ and $G_2 = 1.2$, which verify the ULS CV entanglement in our system. The abscissa numbers 1–7 represent seven possible bipartitions of each wave packet unit and the ordinate N within the range of [1, 20 399] represents the index of wave packet unit. From Fig. 2(a), we can see that all these smallest symplectic eigenvalues v are smaller than 1 for the arbitrary value of N, which demonstrates the existence of entanglement in each wave packet unit. Therefore, these results demonstrate the generation of the ULS CV quantum entanglement containing $2\times 20\,400$ wave packets in our system. To observe the distribution of seven smallest symplectic eigenvalues v of each wave packet unit more clearly, we plotted the v of the first wave packet unit ($N = 1$) which contains $\hat{a}^{(4)}_{\mathrm{pr},1}$, $\hat{a}^{(4)}_{\mathrm{conj},1}$, $\hat{a}^{(4)}_{\mathrm{pr},2}$, and $\hat{a}^{(4)}_{\mathrm{conj},2}$ when $G_1 = 1.3$ and $G_2 = 1.2$ in Fig. 2(b). We can see that the green bar is the highest one in Fig. 2(b), meaning that the subsystem of ($\hat{a}^{(4)}_{\mathrm{pr},1}$, $\hat{a}^{(4)}_{\mathrm{conj},1}$) is relatively weakly entangled to the subsystem of ($\hat{a}^{(4)}_{\mathrm{pr},2}$, $\hat{a}^{(4)}_{\mathrm{conj},2}$), compared with other bipartitions. In addition, we find that there is quantum entanglement between six, eight, and ten wave packets.

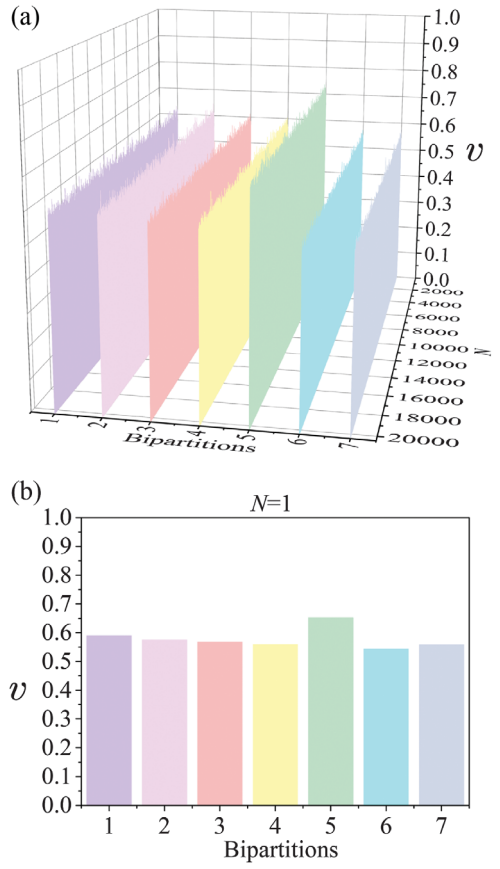

FIG. 2. Witnessing the ULS CV quantum entanglement. (a) Measured smallest symplectic eigenvalues of 20 399 wave packet units when $G_1 = 1.3$ and $G_2 = 1.2$. Seven dfferent colors represent the smallest symplectic eigenvalues v of the seven bipartitions. All the eigenvalues v are less than 1, indicating that each wave packet unit is entangled or inseparable. N represents the wave packet unit index. (b) The corresponding results of the first wave packet unit ($N = 1$).

In order to further study the quantum property of the generated ULS quantum entanglement, it is also useful to reveal its eigenmode decomposition by diagonalizing the CM [25,48]. Figure 3 shows the eigenmodes and their corresponding eigenvalues of the CM of the first wave packet unit when $G_1 = 1.3$ and $G_2 = 1.2$. For amplitude quadrature, the first eigenmode of $0.46\hat{X}^{(4)}_{\mathrm{pr},1} - 0.59\hat{X}^{(4)}_{\mathrm{conj},1} + 0.42\hat{X}^{(4)}_{\mathrm{pr},2} - 0.51\hat{X}^{(4)}_{\mathrm{conj},2}$ has a squeezing level or eigenvalue of -3.28 dB. Meanwhile, the third eigenmode of $-0.32\hat{X}^{(4)}_{\mathrm{pr},1} + 0.58\hat{X}^{(4)}_{\mathrm{conj},1} + 0.38\hat{X}^{(4)}_{\mathrm{pr},2} - 0.64\hat{X}^{(4)}_{\mathrm{conj},2}$ has a squeezing level of -1.35 dB. We can also see that the phase quadrature squeezed eigenmodes are the second eigenmode $0.35\hat{Y}^{(4)}_{\mathrm{pr},1} + 0.34\hat{Y}^{(4)}_{\mathrm{conj},1} + 0.48\hat{Y}^{(4)}_{\mathrm{pr},2} + 0.73\hat{Y}^{(4)}_{\mathrm{conj},2}$ and the fourth eigenmode $-0.38\hat{Y}^{(4)}_{\mathrm{pr},1} - 0.80\hat{Y}^{(4)}_{\mathrm{conj},1} + 0.34\hat{Y}^{(4)}_{\mathrm{pr},2} + 0.33\hat{Y}^{(4)}_{\mathrm{conj},2}$ with squeezing levels of -3.41 and -1.47 dB, respectively. It can be found that the other

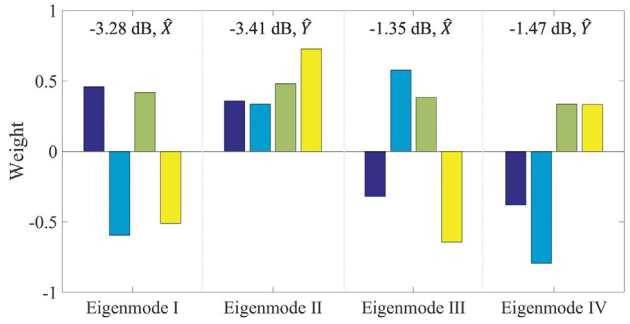

FIG. 3. Eigenmodes and the corresponding squeezing levels of the first output wave packet unit retrieved from CM when $G_1 = 1.3$ and $G_2 = 1.2$. Eigenmode I and eigenmode III are amplitude quadrature squeezed while eigenmode II and eigenmode IV are phase quadrature squeezed. The height of bars represents the relative weight of modes $\hat{a}^{(4)}_{\mathrm{pr},1}$, $\hat{a}^{(4)}_{\mathrm{conj},1}$, $\hat{a}^{(4)}_{\mathrm{pr},2}$, and $\hat{a}^{(4)}_{\mathrm{conj},2}$ for each eigenmode.

20 398 wave packet units have similar eigenmode structures and eigenvalues. In other words, each wave packet unit of the generated ULS quantum entanglement has four independent squeezed modes. Therefore, in total, we have 81 596 squeezed modes for the whole ULS entangled state. For the purpose of verifying the consistency of the squeezing levels of the eigenmodes for these 20 399 wave packet units, we plot the eigenvalues of these wave packet units in Fig. 4. The detailed distributions of amplitude (phase) quadrature eigenvalues are depicted in regions I (II) and III (IV). There are 20 399 different colors which represent 20 399 different values in each eigenvalue region. The eigenvalues of regions I (III) and II (IV) are similar in numerical value, which is consistent with theoretical prediction.

In conclusion, we have theoretically proposed and experimentally demonstrated a scheme for generating ULS CV deterministic quantum entanglement consisting

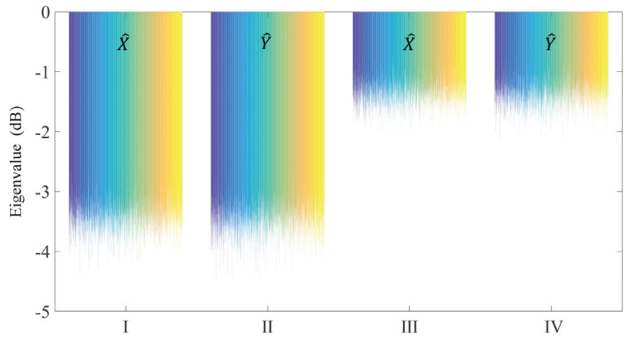

FIG. 4. Eigenvalues of 20 399 consecutive output wave packet units when $G_1 = 1.3$ and $G_2 = 1.2$. The amplitude (phase) quadrature eigenvalues of all output wave packet units are plotted in regions I and III (II and IV). There are 20 399 different colors in regions I–IV, respectively. The eigenvalues are measured in decibels.

of $2 \times 20\,400$ time wave packet optical modes based on a time-delayed SU(1,1) quantum interferometer. Firstly, we demonstrate that all the consecutive wave packet units are entangled by testing all the seven smallest symplectic eigenvalues of 20 399 wave packet units. Then, by retrieving eigenmodes from the CM, we reveal that each wave packet unit is indeed composed of four independent squeezed modes. Therefore, the generated ULS entanglement contains 81 596 squeezed modes. Furthermore, we verify the consistency of the eigenmode squeezing levels for all the wave packet units. The squeezing levels of the eigenmodes are between −3.4 and −1.35 dB. It is limited by the original squeezing level from the entanglement source, optical losses in the setup, and electrical noise from balanced homodyne detector. In the future, if we want to continue to improve the squeezing level, we should reduce the atomic absorption in the vapor cell, the optical losses of the setup, and the electronics noise of the balanced homodyne detector [49]. Because of exploiting of time-delayed SU(1,1) quantum interferometer, the generated ULS quantum entanglement has a different state structure compared with the works of other groups [28–31]. It should be noted that the interaction structure represented by the magenta link in Fig. 1 is extracted from the structure of Eq. (S11) in the Supplemental Material [38], and this structure does not necessarily reflect the structure of the final entangled state. It is also different from the stick representation of the cluster or graph states [28–31]. By applying the phase shift on the modes of the states [30,31] or changing the measurement basis [50], it may be possible to transform the generated state of our scheme into a cluster state. In the future, there are several possibilities to further increase the scalability of our scheme, including exploiting the cascaded FWM processes [51,52], combining with spatial pump shaping technique [27,53], and integrating more degrees of freedom, such as orbital angular momentum and frequency. Because of the large scale and deterministic generation method, our ULS CV quantum entanglement could find applications for implementing ULS CV quantum information processing.

This work was funded by the National Natural Science Foundation of China (12225404, 11874155, 91436211, 11374104, 12174110); Innovation Program of Shanghai Municipal Education Commission (Grant No. 2021-01-07-00-08-E00100); Program of Shanghai Academic Research Leader (22XD1400700); Basic Research Project of Shanghai Science and Technology Commission (20JC1416100); Natural Science Foundation of Shanghai (17ZR1442900); Minhang Leading Talents (201971); Shanghai Sailing Program (21YF1410800); Natural Science Foundation of Chongqing (CSTB2022NSCQ-MSX0893); Shanghai Municipal Science and Technology Major Project (2019SHZDZX01); the 111 project (B12024).

*These authors contributed equally to this work.
†Corresponding author.
ssliu@lps.ecnu.edu.cn
‡Corresponding author.
jtjing@phy.ecnu.edu.cn

[1] A. Einstein, B. Podolsky, and N. Rosen, Phys. Rev. **47**, 777 (1935).
[2] S. L. Braunstein and P. van Loock, Rev. Mod. Phys. **77**, 513 (2005).
[3] D. P. DiVincenzo, Science **270**, 255 (1995).
[4] S. Lloyd and S. L. Braunstein, Phys. Rev. Lett. **82**, 1784 (1999).
[5] D. Gottesman and I. L. Chuang, Nature (London) **402**, 390 (1999).
[6] R. Ukai, N. Iwata, Y. Shimokawa, S. C. Armstrong, A. Politi, J.-i. Yoshikawa, P. van Loock, and A. Furusawa, Phys. Rev. Lett. **106**, 240504 (2011).
[7] R. Ukai, S. Yokoyama, J.-i. Yoshikawa, P. van Loock, and A. Furusawa, Phys. Rev. Lett. **107**, 250501 (2011).
[8] J. Zhang and S. L. Braunstein, Phys. Rev. A **73**, 032318 (2006).
[9] N. C. Menicucci, P. van Loock, M. Gu, C. Weedbrook, T. C. Ralph, and M. A. Nielsen, Phys. Rev. Lett. **97**, 110501 (2006).
[10] A. Furusawa, J. L. Sørensen, S. L. Braunstein, C. A. Fuchs, H. J. Kimble, and E. S. Polzik, Science **282**, 706 (1998).
[11] J.-G. Ren *et al.*, Nature (London) **549**, 70 (2017).
[12] M. Huo, J. Qin, J. Cheng, Z. Yan, Z. Qin, X. Su, X. Jia, C. Xie, and K. Peng, Sci. Adv. **4**, eaas9401 (2018).
[13] S. Liu, Y. Lou, and J. Jing, Nat. Commun. **11**, 3875 (2020).
[14] S. Pirandola, J. Eisert, C. Weedbrook, A. Furusawa, and S. L. Braunstein, Nat. Photonics **9**, 641 (2015).
[15] J. Yin *et al.*, Nature (London) **582**, 501 (2020).
[16] C. F. Roos, M. Chwalla, K. Kim, M. Riebe, and R. Blatt, Nature (London) **443**, 316 (2006).
[17] V. Giovannetti, S. Lloyd, and L. Maccone, Nat. Photonics **5**, 222 (2011).
[18] X. Guo, C. R. Breum, J. Borregaard, S. Izumi, M. V. Larsen, T. Gehring, M. Christandl, J. S. Neergaard-Nielsen, and U. L. Andersen, Nat. Phys. **16**, 281 (2020).
[19] H. S. Zhong, Y. Li, W. Li, L. C. Peng, Z. E. Su, Y. Hu, Y. M. He, X. Ding, W. Zhang, H. Li, L. Zhang, Z. Wang, L. You, X. L. Wang, X. Jiang, L. Li, Y. A. Chen, N. L. Liu, C. Y. Lu, and J.-W. Pan, Phys. Rev. Lett. **121**, 250505 (2018).
[20] X. L. Wang, Y. H. Luo, H. L. Huang, M. C. Chen, Z. E. Su, C. Liu, C. Chen, W. Li, Y. Q. Fang, X. Jiang, J. Zhang, L. Li, N. L. Liu, C. Y. Lu, and J.-W. Pan, Phys. Rev. Lett. **120**, 260502 (2018).
[21] X. Su, A. Tan, X. Jia, J. Zhang, C. Xie, and K. Peng, Phys. Rev. Lett. **98**, 070502 (2007).
[22] Y. Lu, S. Zhang, K. Zhang, W. Chen, Y. Shen, J. Zhang, J.-N. Zhang, and K. Kim, Nature (London) **572**, 363 (2019).
[23] L. Pezzè, M. Gabbrielli, L. Lepori, and A. Smerzi, Phys. Rev. Lett. **119**, 250401 (2017).
[24] Y. Wu *et al.*, Phys. Rev. Lett. **127**, 180501 (2021).
[25] J. Roslund, R. M. de Araujo, S. Jiang, C. Fabre, and N. Treps, Nat. Photonics **8**, 109 (2014).
[26] M. Chen, N. C. Menicucci, and O. Pfister, Phys. Rev. Lett. **112**, 120505 (2014).

[27] W. Wang, K. Zhang, and J. Jing, Phys. Rev. Lett. **125**, 140501 (2020).
[28] S. Yokoyama, R. Ukai, S. C. Armstrong, C. Sornphiphatphong, T. Kaji, S. Suzuki, J.-i. Yoshikawa, H. Yonezawa, N. C. Menicucci, and A. Furusawa, Nat. Photonics **7**, 982 (2013).
[29] J.-i. Yoshikawa, S. Yokoyama, T. Kaji, C. Sornphiphatphong, Y. Shiozawa, K. Makino, and A. Furusawa, APL Photonics **1**, 060801 (2016).
[30] W. Asavanant, Y. Shiozawa, S. Yokoyama, B. Charoensombutamon, H. Emura, R. N. Alexander, S. Takeda, J.-i. Yoshikawa, N. C. Menicucci, H. Yonezawa, and A. Furusawa, Science **366**, 373 (2019).
[31] M. V. Larsen, X. Guo, C. R. Breum, J. S. Neergaard-Nielsen, and U. L. Andersen, Science **366**, 369 (2019).
[32] B. Yurke, S. L. McCall, and J. R. Klauder, Phys. Rev. A **33**, 4033 (1986).
[33] J. Jing, C. Liu, Z. Zhou, Z. Y. Ou, and W. Zhang, Appl. Phys. Lett. **99**, 011110 (2011).
[34] F. Hudelist, J. Kong, C. Liu, J. Jing, Z. Y. Ou, and W. Zhang, Nat. Commun. **5**, 3049 (2014).
[35] C. M. Caves, Adv. Quantum Technol. **3**, 1900138 (2020).
[36] A. Kumar, H. Nunley, and A. M. Marino, Phys. Rev. A **95**, 053849 (2017).
[37] A. M. Marino, V. Boyer, and P. D. Lett, Phys. Rev. Lett. **100**, 233601 (2008).
[38] See Supplemental Material at http://link.aps.org/supplemental/10.1103/PhysRevLett.130.060801 for the interaction structure of generated states, definition of independent wave packet, balanced homodyne detection technique, phase locking of quantum interferometer, and the vacuum locking technique, which includes Refs. [39,40].
[39] O. Morin, K. Huang, J. Liu, H. L. Jeannic, C. Fabre, and J. Laurat, Nat. Photonics **8**, 570 (2014).
[40] Y. Cai, J. Roslund, V. Thiel, C. Fabre, and N. Treps, npj Quantum Inf. **7**, 82 (2021).
[41] V. Boyer, A. M. Marino, R. C. Pooser, and P. D. Lett, Science **321**, 544 (2008).
[42] A. S. Coelho, F. A. S. Barbosa, K. N. Cassemiro, A. S. Villar, M. Martinelli, and P. Nussenzveig, Science **326**, 823 (2009).
[43] R. Simon, Phys. Rev. Lett. **84**, 2726 (2000).
[44] F. A. S. Barbosa, A. S. Coelho, A. J. de Faria, K. N. Cassemiro, A. S. Villar, P. Nussenzveig, and M. Martinelli, Nat. Photonics **4**, 858 (2010).
[45] R. F. Werner and M. M. Wolf, Phys. Rev. Lett. **86**, 3658 (2001).
[46] K. N. Cassemiro and A. S. Villar, Phys. Rev. A **77**, 022311 (2008).
[47] K. Huang, H. Le Jeannic, J. Ruaudel, O. Morin, and J. Laurat, Rev. Sci. Instrum. **85**, 123112 (2014).
[48] C. Fabre and N. Treps, Rev. Mod. Phys. **92**, 035005 (2020).
[49] H. Vahlbruch, M. Mehmet, K. Danzmann, and R. Schnabel, Phys. Rev. Lett. **117**, 110801 (2016).
[50] Y. Cai, J. Roslund, G. Ferrini, F. Arzani, X. Xu, C. Fabre, and N. Treps, Nat. Commun. **8**, 15645 (2017).
[51] S. Li, X. Pan, Y. Ren, H. Liu, S. Yu, and J. Jing, Phys. Rev. Lett. **124**, 083605 (2020).
[52] L. Cao, J. Qi, J. Du, and J. Jing, Phys. Rev. A **95**, 023803 (2017).
[53] K. Zhang, W. Wang, S. Liu, X. Pan, J. Du, Y. Lou, S. Yu, S. Lv, N. Treps, C. Fabre, and J. Jing, Phys. Rev. Lett. **124**, 090501 (2020).